Title

Nonlinear Drive of Tearing Mode by Microscopic Plasma Turbulence

Journal

Plasma and Fusion Research, 2(0)

ISSN

1880-6821

Authors

YAGI, Masatoshi
ITOH, Sanae-I
ITOH, Kimitaka
et al.

Publication Date

2007

DOI

10.1585/pfr.2.025

Peer reviewed

Nonlinear Drive of Tearing Mode by Microscopic Plasma Turbulence

Masatoshi YAGI, Sanae-I. ITOH, Kimitaka ITOH[1)], Masafumi AZUMI[2)], Patrick H. DIAMOND[3)], Atsushi FUKUYAMA[4)] and Takayuki HAYASHI

Research Institute for Applied Mechanics, Kyushu University, Fukuoka 816-8580, Japan
[1)]*National Institute for Fusion Science, Toki 509-5292, Japan*
[2)]*Center for Promotion of Computational Science and Engineering, Japan Atomic Energy Agency, Tokyo 110-0015, Japan*
[3)]*Physics Department, University of California San Diego, CA 92093-0354, USA*
[4)]*Department of Nuclear Engineering, Kyoto University, Kyoto 606-8501, Japan*

(Received 1 March 2007 / Accepted 24 April 2007)

The dynamics of the tearing mode and microscopic resistive drift wave turbulence are studied by performing a nonlinear simulation based on a 4-field Reduced MHD model, placing an emphasis on the interaction between microscopic and transport processes. The simulation results show the importance of turbulent fluctuations for the onset of the tearing mode. The faster growth of microscopic fluctuations induces accelerated growth of the tearing mode, which is much faster than the linear growth rate. A turbulence-driven magnetic island is formed. This is based on the incoherent emission of the long wavelength mode by microscopic turbulence.

Keywords: tearing mode, resistive drift wave, beat interaction, weak turbulence, neoclassical tearing mode, multi-scale simulation

DOI: 10.1585/pfr.2.025

1. Introduction

Magnetized plasmas are nonuniform and exist in a state far from thermal equilibrium. Consequently, in such plasmas various kinds of bifurcations could appear followed by an abrupt change of the topological structure of the magnetic field, examples being sawtooth oscillation and neoclassical tearing modes (NTM). Much work has been done for NTM [1,2], but its trigger conditions remain unclear. Turbulence, as well as the neoclassical transport effect, might play roles in driving NTM. The hierarchical interaction between turbulence and MHD modes is an important issue in tokamak physics [3]. One key process is the role of turbulence's coherent effect on the global mode. Examples of coherent interaction among different scale-length dynamics include process of generating the zonal flow and zonal field, which has been recently reviewed [4]. Another example is a possible enhancement of the resistivity owing to background turbulence, which may increase the growth rate of resistive turbulence. The other key process is an incoherent generation of large-scale perturbation by microscopic fluctuations. For instance, the nonlinear interaction of microscopic turbulence has been pointed out to cause a stochastic onset of the neoclassical tearing mode in the case of linearly stable plasmas. Such a theoretical analysis shows the need for direct simulations in the study of this important subject.

In the present paper, we investigate the dynamics of the tearing modes and resistive drift wave turbulence simultaneously, based on a 4-field Reduced Magneto Hydro Dynamics (RMHD) model. In the simulation study, emphasis is placed on the interactions between the tearing mode, microscopic fluctuations, and transport processes. The transition from the tearing mode to a quasi-mode is found to be induced by drift wave turbulence, and the growth rate is accelerated [5]. This generates a seed magnetic island for the tearing mode. An analytical study is performed based on the weak turbulence theory. An explanation of the accelerated growth rate is given, and the generated island is discussed. This turbulence-induced seed island can play an important role for the trigger of the linearly-stable NTM.

2. Model

In this paper, the nonlinear evolution of NTM in the presence of drift wave turbulence is investigated using a set of 4-field RMHD equations, where the fluctuating ion parallel flow and neoclassical ion viscosity are taken into account [1, 6]. In this system, the electric resistivity and the neoclassical Bootstrap current destabilizes the perturbations in the range of drift wave frequencies, as has been shown in, e.g.,[7]. In the previous study, a linear analysis of the tearing mode (TM) with neoclassical viscosity has been performed using a 3-field model and has been compared with the one using a 4-field model. It was found that both the parallel compressibility and the neoclassical ion viscosity in the 4-field model stabilize the TM, even though $\Delta' > 0$ in the banana regime [6]. Inclusion of an

author's e-mail: yagi@riam.kyushu-u.ac.jp

ion temperature evolution equation in the system, i.e., a 5-field model, will allow the coupling between the NTM and ITG mode turbulence.

The quantities $\{\phi, A, v, p\}$, which are chosen as dynamical variables, are the fluctuating electrostatic potential, the vector potential parallel to the magnetic field, parallel velocity, and electron density. The model equations are written as

$$\frac{\partial}{\partial t}\nabla_\perp^2 F + [F, \nabla_\perp^2 F] - \alpha_\mathrm{i}\nabla_\perp \cdot [p, \nabla_\perp F] = -\nabla_{//}\nabla_\perp^2 A + \mu_\mathrm{i}^\mathrm{c}\nabla_\perp^4 F - \frac{q_\mathrm{s}}{\varepsilon_\mathrm{s}}\mu_\mathrm{i}^\mathrm{nc}\frac{\partial U_\mathrm{pi}}{\partial r} - \frac{q_\mathrm{s}}{\varepsilon_\mathrm{s}}\frac{m_\mathrm{e}}{m_\mathrm{i}}\mu_\mathrm{e}^\mathrm{nc}\frac{\partial U_\mathrm{pe}}{\partial r}, \quad (1)$$

$$\frac{\partial}{\partial t}A = -\nabla_{//}(\phi - \alpha_\mathrm{e}p) + \eta_{//}^\mathrm{c}\nabla_\perp^2 A + \alpha\frac{m_\mathrm{e}}{m_\mathrm{i}}\mu_\mathrm{e}^\mathrm{nc}U_\mathrm{pe}, \quad (2)$$

$$\frac{\mathrm{d}v}{\mathrm{d}t} = -\nabla_{//}p + 4\mu_\mathrm{i}^\mathrm{c}\nabla^2 v - \mu_\mathrm{i}^\mathrm{nc}U_\mathrm{pi} - \frac{m_\mathrm{e}}{m_\mathrm{i}}\mu_\mathrm{e}^\mathrm{nc}U_\mathrm{pe}, \quad (3)$$

$$\frac{\mathrm{d}p}{\mathrm{d}t} = -\hat{\beta}\nabla_{//}(v + \alpha\nabla_\perp^2 A) + \hat{\beta}\eta_\perp^\mathrm{c}\nabla_\perp^2 p - \hat{\beta}\alpha\frac{m_\mathrm{e}}{m_\mathrm{i}}\frac{q_\mathrm{s}}{\varepsilon_\mathrm{s}}\mu_\mathrm{e}^\mathrm{nc}\frac{\partial U_\mathrm{pe}}{\partial r}, \quad (4)$$

where $F = \phi + \alpha_\mathrm{i}p$ is the generalized potential, $U_\mathrm{pi} = v + (q_\mathrm{s}/\varepsilon_\mathrm{s})\partial F/\partial r$ and $U_\mathrm{pe} = v + \alpha\nabla_\perp^2 A + (q_\mathrm{s}/\varepsilon_\mathrm{s})\partial/\partial r(F - \alpha p)$ are the fluctuating neoclassical ion and electron flows, respectively, $\mathrm{d}/\mathrm{d}t = \partial/\partial t + [\phi,]$, $\nabla_{//} = \partial/\partial z - [A,]$ and $[,]$ is the Poisson bracket. In this model, the ion and electron temperatures are assumed to be constant. The coefficients $\{\mu_\mathrm{i}^\mathrm{cl}, \eta_{//}^\mathrm{cl}, \eta_\perp^\mathrm{cl}\}$ are classical ion viscosity, parallel and perpendicular resistivity [8]. The normalization $v_\mathrm{A}t/R \to t$, $r/a \to r$ is adapted, where v_A is the Alfven velocity, R is the major radius, and a is the minor radius. Other parameters are defined by $\hat{\beta} = \beta/(1+\beta)$, $\alpha = c/(a\omega_\mathrm{pi})$, $\alpha_\mathrm{i} = \alpha/(1+\tau)$, $\alpha_\mathrm{e} = \tau\alpha/(1+\tau)$ with plasma beta β, the speed of light c, ion plasma frequency ω_pi, and the ratio of electron to ion temperature $\tau = T_\mathrm{e}/T_\mathrm{i}$. The subscript 's' in the safety factor q_s and the inverse aspect ratio ε_s indicate the value evaluated at the resonance surface.

This model conserves the energy in the dissipationless limit [9, 10]. The energy balance in the system is given by

$$\frac{\mathrm{d}H}{\mathrm{d}t} = -\int \mathrm{d}V \left(\mu_\mathrm{i}^\mathrm{c}|\nabla_\perp^2 F|^2 + \eta_{//}^\mathrm{c}|\nabla_\perp^2 A|^2 + 4\mu_\mathrm{i}^\mathrm{c}|\nabla_\perp v|^2 + \eta_\perp^\mathrm{c}|\nabla_\perp p|^2 + \mu_\mathrm{i}^\mathrm{nc}|U_\mathrm{pi}|^2 + \frac{m_\mathrm{e}}{m_\mathrm{i}}\mu_\mathrm{e}^\mathrm{nc}|U_\mathrm{pe}|^2\right) \quad (5)$$

with

$$H = \frac{1}{2}\int \mathrm{d}V \left(|\nabla_\perp F|^2 + |\nabla_\perp A|^2 + |v|^2 + \frac{|p|^2}{\hat{\beta}}\right). \quad (6)$$

In Eq. (6), the first term in RHS represents the electrostatic energy, the second term the electromagnetic energy, the third term the ion kinetic energy parallel to the ambient magnetic field, and the fourth term internal energy.

The model of neoclassical viscosity is key for the study of the tearing mode. The neoclassical viscosities are given by the interpolated formula [11] as

$$\mu_\mathrm{e}^\mathrm{nc} = \frac{2.3\sqrt{\varepsilon}\nu_\mathrm{e}}{(1 + 1.07\nu_{\mathrm{e}^*}^{1/2} + 1.02\nu_{\mathrm{e}^*})(1 + 1.07\varepsilon^{3/2}\nu_{\mathrm{e}^*})}, \quad (7)$$

$$\mu_\mathrm{i}^\mathrm{nc} = \frac{0.66\sqrt{\varepsilon}\nu_\mathrm{i}}{(1+1.03\nu_{\mathrm{i}^*}^{1/2}+0.31\nu_{\mathrm{i}^*})(1+0.66\varepsilon^{3/2}\nu_{\mathrm{i}^*})}, \quad (8)$$

where $\nu_{\mathrm{i,e}^*} = \nu_{\mathrm{i,e}}/(\varepsilon^{3/2})(qR)/v_{\mathrm{thi,e}}$. It should be noted that this set of equations with toroidal curvature terms in the vorticity equation and in the electron density equation was used for analyzing the neoclassical ballooning mode in the fluid limit [12]. Without neoclassical viscosity, these equations agree with those originally derived by Hazeltine *et al.* [9]. Microscopic instabilities, which we refer to here simply as 'resistive drift waves', have sometimes been referred to as 'the neoclassical pressure-gradient-driven MHD turbulence' when the role of the neoclassical Bootstrap current ($\mu_\mathrm{e}^\mathrm{nc}U_\mathrm{pe}$ term in Eq. (2)) is illuminated in the destabilization mechanisms [7].

For simplicity, we keep only the convective nonlinearity and neglect the gyro-viscous nonlinearity in Eq. (1):

$$[F, \nabla_\perp^2 F] - \alpha_\mathrm{i}\nabla \cdot [p, \nabla_\perp F] = [\phi, \nabla_\perp^2 F] - \frac{\alpha_\mathrm{i}}{r}p_0'''\frac{\partial\phi}{\partial\theta} + \alpha_\mathrm{i}\left(\frac{p_0'}{r}\right)'\frac{1}{r}\frac{\partial F}{\partial\theta} - \frac{\alpha_\mathrm{i}}{r}p_0''\frac{\partial^2 F}{\partial r\partial\theta} + \text{gyro-vis. non.} \quad (9)$$

It is found that this nonlinearity leads to a strong normal cascade of energy. This influence is important for the level of turbulence saturation [10], but it weakly affects the saturation of the magnetic island. The details of this effect will be reported elsewhere.

3. Parameters and Linear Stability

The model q profile and pressure profile

$$q(r) = q_1(1 + (r/r_\mathrm{s})^a)^b + q_2, \quad q_1 = (q_\mathrm{s} - q_0)/(2^b - 1), \quad q_2 = q_0 - q_1 \quad (10)$$

and $p(r) = (\beta/\varepsilon)(1 - r^2)^2$ are introduced. Parameters are chosen as $q_\mathrm{s} = 2$, $a = 3$, $b = 1$, $\varepsilon = 1/3$, $\beta = 0.01$, $\alpha = 0.01$, and $\tau = 1$. For nonlinear simulation, we use $\eta_{//}^\mathrm{c} = 10^{-5}$. This large resistivity number is due to the limitation of computation, but casts an issue for the excitation of microscopic modes. If we use formulas (7) and (8) (the HS model), the neoclassical viscosity corresponds to the one in the Pfirsh-Schluter regime for $\eta_{//}^\mathrm{c} = 10^{-5}$. To avoid this situation, we use the model with enhanced neoclassical viscosity (the B model) given by $\mu_\mathrm{e}^\mathrm{nc} = 2.3\sqrt{\varepsilon}\nu_\mathrm{e}$, $\mu_\mathrm{i}^\mathrm{nc} = 0.66\sqrt{\varepsilon}\nu_\mathrm{i}$ instead of Eqs. (7) and (8). These models are briefly explained in Fig. 1 in Ref. [5].

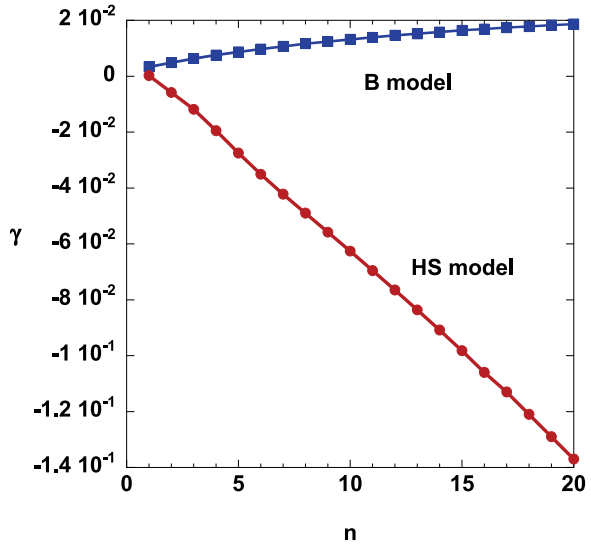

Fig. 1 Linear growth rate versus toroidal mode number n in HS and B models.

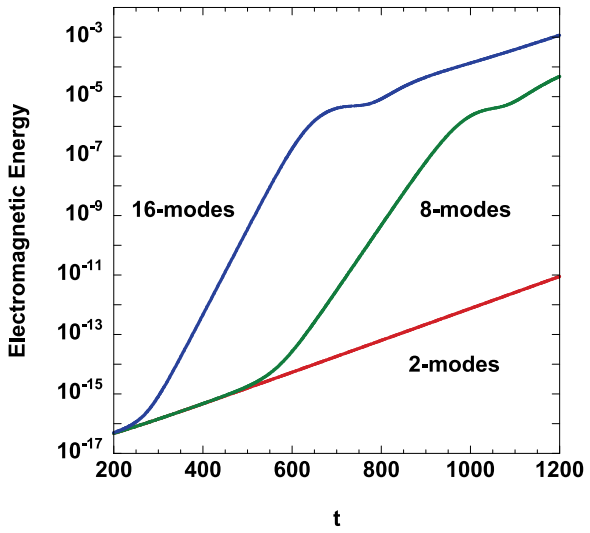

Fig. 2 Time evolution of electromagnetic energy of the (2,1) mode for cases with various Fourier modes.

Figure 1 shows the dependence of the linear growth rate on the toroidal mode number n for the HS model and the B model with $q_0 = 1.01$ and $r_s = 0.56$. For the HS model, only the (2,1) mode is unstable (classical TM), while on the other hand, for the B model, the linear growth rate increases with increases in the mode number. In this regime, the result shown in Fig. 1 satisfies the relation

$$\gamma \propto R_M^{-1/3} n^{0.6}, \tag{11}$$

for which the result of an analytic theory [7]

$$\gamma \propto R_M^{-1/3} n^{2/3} \tag{12}$$

is considered to be relevant (R_M: the Magnetic Reynolds number). Note that additional mechanisms (e.g., the neoclassical effect in Eq. (1)) also work in the present model. For modes with large mode numbers ($n > 30$), the growth rate decreases owing to the collisional diffusion effect (see Fig. 2 in Ref. [5]). The details of linear mode stability will be reported elsewhere [13].

We also investigate the dependence of the q profile on the growth rate. In this study, we could not find the window where $\Delta'_{2,1}$ is negative while there exists unstable collisional drift wave in high-n regime, which is suitable for the demonstration of the nonlinear excitation of NTM by turbulence. In this paper, we discuss the case with $q_0 = 1.2$ and $r_s = 0.6$ with $\Delta'_{2,1} \equiv (A'_{2,1}(r_s + 0) - A'_{2,1}(r_s - 0))/A_{2,1}(r_s) = 10.25$. Under this circumstance, there is no subcritical excitation of NTM, but the defect of bootstrap current on the island can destabilize the mode. In addition, multi-scale interaction between the TM mode and turbulence are explicitly demonstrated in nonlinear simulations.

4. Nonlinear Simulation

4.1 Acceleration of the growth of the tearing mode

The nonlinear simulation with single helicity modes is performed using a spectral code. The boundary condition is given by $f_{m,n}(0) = f_{m,n}(1) = 0$ and $f'_{0,0}(0) = 0$, $f_{0,0}(1) = 0$. Figure 2 shows the time evolution of the electromagnetic energy of the (2,1) mode for cases with different Fourier modes in the spectral space. Here, the '2-modes' indicates (2,1), (4,2), these complex conjugate and (0,0) modes. Similarly, the '8-modes' means (2,1), (4,2), ..., (16,8), these complex conjugate and (0,0) modes. The 2-modes case indicates the dynamics of the tearing mode, i.e., the (2,1) mode in the presence of the back-interaction of the quasilinear profile modification. The well-known linear growth of the tearing mode and saturation are obtained. If the evolution of the microscopic fluctuations is simultaneously solved, it is newly found that nonlinear acceleration occurs in the early growing phase. However, saturation amplitude is weakly affected by high-n modes.

4.2 Time evolution of TM in the growing phase

The aim of this study is to investigate what nonlinear mechanisms cause the sudden acceleration of the growth rate of the TM. First examined is the role of the quasilinear background profile modification. We next investigate the influence of the zonal field. Following this, the effect of nonlinear incoherent emission from microfluctuations is investigated.

The role of background profile modification is studied. A reference calculation was performed, in which the quasilinear effect is turned off. (In other words, nonlinear terms for the evolution of the (0,0) mode are set to be zero.) The case with the QL effect and that without are compared.

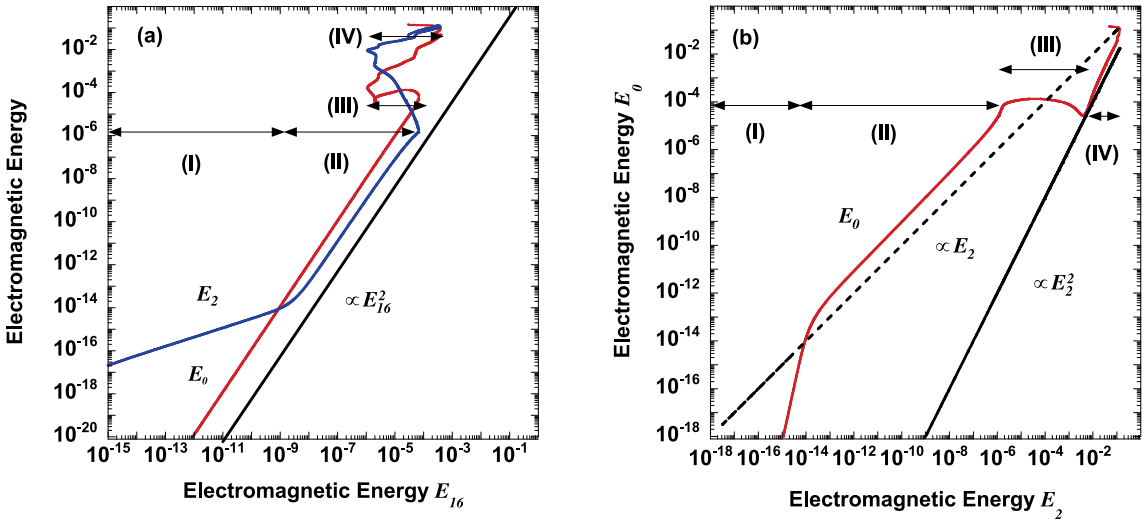

Fig. 3 Lissajous curve showing the relation between microscopic fluctuations and macroscopic perturbations (a). Relation between the (2,1) mode energy and that of the (0.0) mode (b).

It was concluded that the accelerated growth of the tearing mode occurs in both simulations. That is, the accelerated growth of the tearing mode in the presence of microfluctuations is not induced by the QL effect. (Of cause, the QL effect is quite important for saturation phase.)

In order to study the magnitude of the drive from microturbulence to the global perturbations, a Lissajous curve is shown in Fig. 3 (a), corresponding to the case with 8-modes shown in Fig. 2. Figure 3 (a) draws (E_{16}, E_2) and (E_{16}, E_0), where E_{16} is the energy of the $(m, n) = (16, 8)$ mode, E_2 is that of the (2, 1) mode, and E_0 is the one for the (0, 0) component, respectively. This figure shows that there are four phases. That is, in the first phase, the high-mode number energy E_{16} increases much faster than the growth of E_2. In the next phase, a quadratic dependence of E_2 with respect to E_{16} holds, i.e., a relation

$$E_2 \propto E_{16}^2 \tag{13a}$$

is found. In the first (I) and second phase (II), a quadratic relation $E_0 \propto E_{16}^2$ holds. In the third phase (III), E_{16} decreases but E_2 continues to rise. In the last phase (IV), both E_2 and E_0 increase. It is also shown in figure 3 (b) that

$$E_0 \simeq E_2 \tag{13b}$$

holds in the phase (II), but $E_0 \propto E_2^2$ is satisfied in the phase (IV). This means that, in the last phase (IV), the change of the energy of the (0, 0) component is induced by the quasilinear effect of the (2, 1) tearing mode.

The relation (13a) shows the essential feature of the accelerated growth of the tearing mode. In phases (I) and (II), the microscopic fluctuations show the exponential growth, which is symbolically written as

$$I_{\text{high } m} \propto \exp(\gamma_h t). \tag{14}$$

The relation by Eq. (13a) indicates that the accelerated growth of the tearing mode can be described by the relation

$$I_{2/1} \propto \exp(2\gamma_h t), \tag{15}$$

as can the (0, 0) component, $I_{0/0} \propto \exp(2\gamma_h t)$.

In the phase of accelerated growth of the (2,1) mode, this mode behaves as a quasi-mode which is driven by the beating of microscopic perturbations. Figure 4 shows the time evolution of mode frequency in the acceleration phase. In the first phase, $t < 700$, the modes obey the linear response. The deviation of the evolution of the (2,1) mode from linear growth is noticeable for $800 < t$ based on the evolution of the electromagnetic energy. The deviation of the real frequency from the linear phase occurs earlier, $700 < t$, and the (2,1) mode starts to rotate in the direction of the diamagnetic drift. When the transition from the linear phase to the nonlinearly-accelerated phase is completed, $950 < t$, the real frequency tends to satisfy the frequency's matching condition. The frequency of the (2,1) mode in $1040 \leq t \leq 1200$ is found to satisfy

$$\omega_2 \sim \omega_{16} - \omega_{14}, \tag{16}$$

where $\omega_2, \omega_{14}, \omega_{16}$ are the angular frequencies of the (2,1) mode, the (14,7) mode, and the (16,8) mode, respectively. (It is noted that the high-m drift waves have a weak dispersion so that the matching relation $\omega_2 \sim \omega_{m+2} - \omega_m$ holds for other values of m for drift wave components.) This matching condition continues to be satisfied, approximately, after the acceleration of the growth is terminated, $1200 \leq t \leq 1400$. The frequency matching and the matching of the mode numbers suggest that the accelerated growth of the tearing mode is due to the incoherent emission from short wave length turbulence.

The radial wave structure changes from the tearing mode to the localized mode in the phase of accelerated growth due to the turbulent noise. When the microscopic

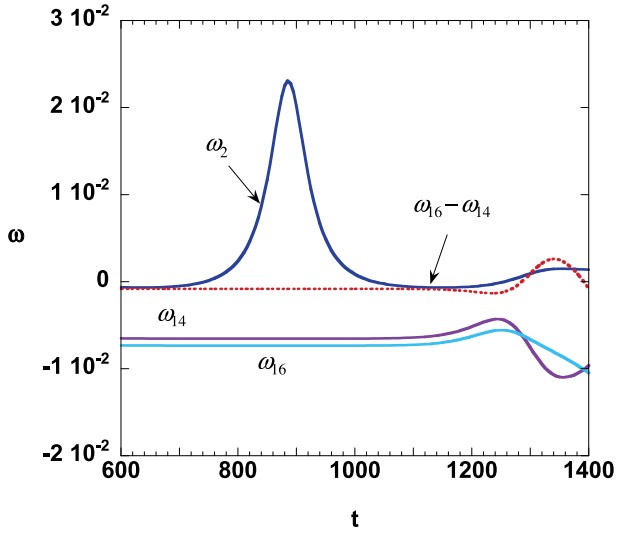

Fig. 4 Time evolution of mode frequency: the (2,1) made (blue), the (16,8) mode (light blue), and the (14,7) mode (purple) are shown. The beat frequency $\omega_{16/8} - \omega_{14/7}$ is shown by the dotted line (red).

fluctuations reach the stationary turbulent state, the (2,1) mode changes from the localized mode to the nonlinear TM. The driven perturbation of the (2,1) mode provides a seed island. We note that the amplitude of the (2,1) mode energy is approximately $10^{-5} \sim 10^{-4}$ of those at saturation when the enhanced growth ends. This means that the island width, which is induced by the nonlinear interaction with the microscopic turbulence, can reach a few percent of the saturation level when the accelerated growth ends. This nonlinear acceleration process is effective in generating a seed island.

Before closing this section, we discuss the nonlinear effects of drift wave fluctuations on the (2,1) mode. Using the partially linearized model, the effects of each nonlinear term are investigated (see Fig. 6 in Ref. [5]). A comparison leads us to the following finding. (i) The acceleration of the growth rate is due to the pump by the high (m, n) modes via nonlinear terms. (ii) The nonlinear terms in any of Eqs. (1) - (4) are sufficient to cause acceleration of the growth rate. (iii) Nonlinearities in the fluctuating density and Ohm's law contribute the strongest to this acceleration. (iv) The termination of this acceleration is due to the termination of the growth of the microscopic fluctuations. When the nonlinear terms in Ohm's law and the vorticity equation are neglected, microfluctuations do not reach stationary turbulence in this simulation. This leads to the continued amplification of the (2,1) mode.

5. Theoretical Analysis

5.1 Weak turbulence formalism

The accelerated growth in the simulation and the sustainment of the turbulence-driven island are studied in the framework of the weak turbulence theory (WTT).

The set of model Eqs. (1) - (4) is formally written as

$$\frac{\partial}{\partial t}\boldsymbol{X} + \boldsymbol{L}\boldsymbol{X} = \boldsymbol{N}, \tag{17}$$

where $\boldsymbol{X} = (F, A, V, P)$, $\boldsymbol{L}$ is the linear operator that determines the linear stability, and $\boldsymbol{N}$ stands for the nonlinear interaction terms. Here, we are interested in the drive of the long-wavelength mode by the beat of microscopic modes. For instance, $X_{k'}$ and $X_{k''}$ are chosen as microscopic fluctuations, which have frequencies $\omega_{k'}$ and $\omega_{k''}$, respectively. The response of the perturbation with

$$\boldsymbol{k} = \boldsymbol{k}' - \boldsymbol{k}'' \tag{18}$$

is considered. (The wave vector $\boldsymbol{k}$ refers to the global mode, and $\boldsymbol{k}'$ and $\boldsymbol{k}''$denote microscopic modes.) In this case, the right hand side of Eq. (17) has the frequency

$$\omega_{\mathrm{b}} = \omega_{k'} - \omega_{k''}. \tag{19}$$

The operator $\boldsymbol{L}$ includes radial derivatives. Formally, $\boldsymbol{L}$ can be expanded in a series of radial eigenfunctions. Instead, theoretical evaluation is performed by simply taking the least stable mode near the frequency ω_{b} at $\boldsymbol{k} = \boldsymbol{k}' - \boldsymbol{k}''$. Thus the operator $\boldsymbol{L}$ is replaced by the matrix $\boldsymbol{L}_k$, which is composed of numerical coefficients. The matrix $\boldsymbol{L}_k$ is diagonalized by use of a unitary matrix as

$$\boldsymbol{U}\boldsymbol{L}_k\boldsymbol{U}^{-1} = \boldsymbol{D}_k, \tag{20}$$

where the diagonal matrix is chosen such that the (1,1) element has the smallest real part (i.e., the least stable mode), and (2, 2) - (4, 4) elements correspond to more stable modes. The response field $\boldsymbol{X}_k$ and the source nonlinear term $\boldsymbol{N}_k$ are also transformed as

$$\boldsymbol{Y}_k = \boldsymbol{U}\boldsymbol{X}_k \ \text{ and } \ \boldsymbol{M}_k = \boldsymbol{U}\boldsymbol{N}_k. \tag{21}$$

Here, for the purpose of analytical insight, we employ two simplifications. First, we study the coupling through the incoherent terms on the right-hand side. The coherent part (which may contribute to the turbulent viscosity and resistivity, etc.) is not considered. If the effects of the coherent interaction are studied, they can be renormalized in the operator $\boldsymbol{L}_k$. Second, we analyze the evolution of the least-stable response $Y_{1,k}$. More strongly damped components, $Y_{n,k}$ $(n = 2, 3, 4)$, are neglected. (Components with larger damping rates $(n = 2, 3, 4)$ can be solved in a similar way, but their contribution to quantity $\boldsymbol{X}_k$ is small due to their larger damping rate.) Following the standard procedure prescribed by the weak turbulence theory [14], which is illustrated in the Appendix, the evolution equation of the perturbation intensity is obtained as

$$\frac{\partial}{\partial t} I_k + \mathrm{Re} D_{11,k}\, I_k = \pi \left| M_{1,k} \right|^2, \tag{22}$$

where $I_k = \int \left| Y_{1,k} \right|^2 \mathrm{d}\omega$.

The nonlinear driving term $M_{1,k} = \sum_{j=1}^{4} U_{1j}N_j$ has absolute value

$$\left|M_{1,k}\right|^2 = \sum_{j,\,j'}^{3} U_{1j}U^*_{1\,j'}N_jN^*_{j'}. \tag{23}$$

As has been demonstrated by the direct nonlinear simulation [5], the nonlinear interaction in one equation is sufficient to induce the accelerated growth in simulations. Thus, we take the most effective nonlinear term N_4, and have a simplified expression as

$$\left|M_{1,k}\right|^2 = \left|U_{14,k}\right|^2 \left|N_{4,k}\right|^2. \tag{24}$$

The nonlinear term N_4 has a structure such as

$$N_{4,k} = \sum_{k'} V_{k-k',k'}X_{j,k-k'}X_{j',k'}. \tag{25}$$

Here, in expression of $X_{j,k'}$, the suffix j indicates the field variable (F, A, V, P). The suffix k' denotes the wavevector of the microscopic fluctuations. Analytic expression of $|M_{1,k}|$ (in the limit of $|k'| \gg |k|$) is derived in the Appendix in the case that $X_{j,k'}$ and $X_{j',k'}$ are in phase (which is of present interest) as

$$\left|M_{1,k}\right|^2 \simeq 2\left|U_{14,k}\right|^2 \sum_{k'\omega'} \left|V_{k',k'}\right|^2 \left|X_{j',k'}\right|^2 \left|X_{j,k'}\right|^2. \tag{26}$$

5.2 Excitation of the global mode

The set of Eqs. (22) and (26) are solved to study the evolution of the global mode in the presence of incoherent emissions from microscopic fluctuations. The long-wavelength mode is driven by the source term (RHS) of Eq. (22). The intensity of the test mode (the (2, 1) in the case of simulations, denoted by $\boldsymbol{k}$) is given by a superimposition of the linear mode and the response to the excitation by the turbulence (denoted by $\boldsymbol{k'}$) as

$$I_k = I_k(0)\exp(\gamma_k t) + \exp(\gamma_k t)\int_0^t \mathrm{d}t' \exp(-\gamma_k t')\pi\left|M_{1,k}\right|^2, \tag{27}$$

where $\gamma_k = -\mathrm{Re}D_{11,k}$.

In the initial value problem of nonlinear simulations, which is discussed in section 4, the amplitude of microscopic fluctuations, $\left|X_{j,k'}\right|^2$ and $\left|X_{j',k'}\right|^2$, grows in time exponentially as

$$\left|X_{j,k'}\right|^2 \propto \exp(\gamma_{\mathrm{h}} t),$$

where γ_{h} stands for the growth rate of the amplitude of microscopic perturbations. Thus, the source term grows with the twice growth rate as

$$\left|M_{1,k}\right|^2 \propto \exp(2\gamma_{\mathrm{h}} t). \tag{28}$$

For the case of drift wave turbulence and the tearing mode, the relation $\gamma_{\mathrm{h}} > \gamma_k$ holds. Equation (27) yields the evolution of the intensity of the macroscopic tearing mode as

$$I_k = I_k(0)\exp(\gamma_k t) + \frac{\pi}{2\gamma_{\mathrm{h}} - \gamma_k}\left|M_{1,k}(0)\right|^2 \exp(2\gamma_{\mathrm{h}} t). \tag{29}$$

This result shows the nonlinear growth of the tearing mode. That is, I_k has two components. The first term includes the mode's linear growth rate. The second term corresponds to the contribution of the microscopic fluctuations. The second term has a larger growth rate than does the first term, in the system of drift waves and tearing mode. If the second term in the RHS of Eq. (29) is small, owing to the small initial values of microfluctuations, the first term in the RHS of Eq. (29) is larger than the second term, showing the linear growth of I_k. However, the second term has larger growth rate, and it overcomes the first term. Under this circumstance, I_k has the dependence as

$$I_k \propto \exp(2\gamma_{\mathrm{h}} t). \tag{30}$$

That is, the nonlinear growth rate of the driven tearing mode is given by twice the growth rate of rapidly growing turbulence. Therefore, when nonlinear growth dominates linear growth for I_k, the relation holds between the intensity of background turbulence $I_{k'}$ as

$$I_k \propto I_{k'}^2. \tag{31}$$

These evolutions expressed by Eqs. (30) and (31) are observed in nonlinear simulation, as is illustrated in Figs. 2 and 3.

5.3 Seed island in stationary turbulence

When the background turbulence is in a stationary state, the driving term (RHS of Eq. (22)) remains constant in time. The stationary island can be sustained, for the case of the stable tearing mode, as

$$I_k = \frac{-\pi}{\gamma_k}\left|M_{1,k}\right|^2. \tag{32}$$

Note that the sign of γ_k is negative if the beat mode is stable. Here, we apply the theory of neoclassical-pressure-gradient mode turbulence [7] to the analysis using the system of Eqs. (1) - (4). (Theoretical expression of the turbulent excitation of the tearing mode has also been discussed and the order of magnitude estimate has been given for the case in which the microscopic turbulence is current-diffusive ballooning mode turbulence [15, 16].)

The unitary transformation has the magnitude of the order of unity for perturbations of the present case, where $|\tilde{p}|$ is the largest but other field components have similar relative amplitude. The Lagrange nonlinearity is the key nonlinear process in the theoretical modeling. This ansatz is also confirmed by direct simulation in which one nonlinearity in the set of equations can reproduce the nonlinear acceleration of the tearing mode. The Lagrange nonlinearity for the microscopic perturbations is evaluated based on the decorrelation rate caused by background fluctuations, and the intensity of the source $\left|M_{1,k}\right|^2$ is evaluated from Eq. (26) as

$$\left|M_{1,k}\right|^2 \sim \sum_{k'\omega'} \frac{k^2}{k'^2}\Gamma^2_{k'}X^2_{k'} \sim \frac{k^2}{k'^2}\Gamma_{k'}\sum_{k'} I_{k'}, \tag{33}$$

where $\Gamma_{k'}$ is the nonlinear decorrelation rate of the microscopic perturbation (k') by other microscopic fluctuations (k''), which is defined as $\Gamma_{k'} X_{k'} = \left\langle \sum_{k''\omega''} V_{k'k''} X_{k''} X_{k'} \right\rangle$, and $I_{k'}$ is the intensity of the microfluctuations. An order of magnitude estimate, $I_{k'} = \sum_{\omega'} X_{k'}^2 \sim \Gamma_{k'} X_{k'}^2$, is employed in relating the Fourier component $X_{k'}$ and the fluctuation intensity $I_{k'}$.

The seed island in stationary turbulence is studied based on Eqs. (32) and (33). The analytic theory of the neoclassical pressure gradient-driven turbulence [7] can be applied to the study of the seed island of the tearing mode. Rewriting the decorrelation rate by use of the turbulent diffusion coefficient (eddy viscosity), $\Gamma_{k'} = D_{\rm turb} k'^2$, the source term is simplified as

$$\left|M_{1,k}\right|^2 \sim k^2 D_{\rm turb} \sum_{k'} I_{k'}. \tag{34}$$

By combining Eqs. (32) and (34), one obtains the level of the stationary seed island for the case of the stable tearing mode ($\gamma_k < 0$) as

$$I_k = \frac{-\pi}{\gamma_k} k^2 \, D_{\rm turb} \sum_{k'} I_{k'}. \tag{35}$$

The formula of Eq. (35) describes the enhanced seed island when the parameters approach the marginal stability condition, $\gamma_k \to 0$. In terms of the field variable, the seed magnetic perturbation for the tearing mode is written as

$$\left|\tilde{B}_k\right| \simeq \sqrt{\frac{k^2 \, D_{\rm turb}}{|\gamma_k|}} \left|\tilde{B}_{\rm micro}\right|, \tag{36}$$

where $\tilde{B}_{\rm micro}$ is the amplitude of microscopic magnetic fluctuations.

As is explained in previous sections, the turbulence analyzed in [7] is not completely identical to that in the present nonlinear simulation. Nevertheless, an essential element for the development of microscopic turbulence (i.e., destabilization by the neoclassical Bootstrap current and saturation by the nonlinear transport) was illustrated in [7]. Thus, it is relevant to apply the result of [7] for the present problem in order to achieve an analytic understanding of the problem. The formulae of the turbulent transport coefficient and fluctuation level were given in [7] as

$$D_{\rm turb} \approx \frac{\varepsilon}{q} \beta_{\rm p} \frac{\eta}{\mu_0} \frac{L_{\rm s}}{L_{\rm p}} \zeta, \tag{37}$$

apart from a numerical coefficient of the order of unity, where $L_{\rm s}$ is the magnetic shear length, $L_{\rm p}$ is the pressure gradient scale length, and $\zeta = \mu_{\rm e}^{\rm nc}(\mu_{\rm e}^{\rm nc} + 0.51\nu_{\rm e})^{-1}$ is a coefficient of the order of unity. Fluctuation amplitude was given as

$$\frac{\left|\tilde{B}_{\rm micro}\right|}{B} \sim \left(\frac{\varepsilon}{q}\beta_{\rm p}\right)^{7/6} \zeta^{4/3} \left(\frac{r^2 L_{\rm s}^3}{\left\langle k_\theta'^2 \right\rangle L_{\rm p}^7}\right)^{1/6} R_{\rm M}^{-1/3}. \tag{38}$$

By combining Eqs. (36), (37), and (38), the level of tearing mode amplitude, which is driven by background turbulence, is estimated as

$$\frac{\left|\tilde{B}_k\right|}{B} \sim \sqrt{\frac{k^2\eta}{|\gamma_k|\mu_0}} \left(\frac{\varepsilon_{\rm s}}{q_{\rm s}}\beta_{\rm p}\right)^{5/3} \zeta^{11/6} \left(\frac{r L_{\rm s}^3}{k_\theta' L_{\rm p}^5}\right)^{1/6} R_{\rm M}^{-1/3}. \tag{39}$$

The seed island is shown to be excited by the pressure gradient, through nonlinear interaction with microscopic turbulence. The width of the seed island depends on $|\gamma_k|$ as $w_{\rm seed} \propto |\gamma_k|^{-1/4}$, and has considerable magnitude away from the critical condition for instability.

5.4 Impact on the transition to the Rutherford regime

In the evolution of the tearing mode instability, the transition from the linear regime to the Rutherford regime [17], where the island width grows not exponentially but linearly in time, is essential.

The threshold amplitude, above which the exponential growth turns to the algebraic growth, was derived by comparing the inertia response to the nonlinear force. The critical amplitude has been derived as

$$\left.\frac{\tilde{B}_r}{r_{\rm s} B_\theta'}\right|_{\rm th} \simeq \frac{\sqrt{2\eta_{//}\rho\gamma}}{r_{\rm s} B_\theta}, \tag{40}$$

where ρ is the mass density and γ is the growth rate of the tearing perturbation [17]. In the absence of coupling with the drift wave turbulence, γ is given by the linear growth rate. In this case, threshold amplitude $\tilde{B}_r\big|_{\rm th} (r_{\rm s} B_\theta')^{-1}$ is of the order of $R_{\rm M}^{-4/5}$. (The dependence on Δ' introduces a coefficient of the order of unity, but is suppressed here for the sake of simplicity.) Thus, within the limit of high temperature, rapid growth of the tearing mode stops at low amplitude, then slow increment follows with the time scale of the resistive diffusion time. Excitation by the nonlinear coupling influences this threshold strongly. In the case in which the incoherent emission by drift waves controls the growth of the tearing mode, γ in Eq. (39) is evaluated by (twice) the growth rate of the drift waves. The threshold amplitude to enter the Rutherford regime $\tilde{B}_r\big|_{\rm th} (r_{\rm s} B_\theta')^{-1}$ is then given as $\sqrt{\tau_{\rm A}\gamma R_{\rm M}^{-1}}$. With the help of the estimate Eq. (11), $\gamma \propto R_{\rm M}^{-1/3}$, the relation for the threshold amplitude is obtained as

$$\left.\frac{\tilde{B}_r}{r_{\rm s} B_\theta'}\right|_{\rm th} \propto R_{\rm M}^{-2/3}, \tag{41}$$

showing a weaker dependence on the magnetic Reynolds number. The transition to the Rutherford regime occurs at much higher amplitude (in high temperature plasmas) owing to the nonlinear coupling with drift wave fluctuations.

6. Summary and Discussion

In this article, we studied the nonlinear mechanism which induces accelerated growth of the tearing mode

when microscopic fluctuations are simultaneously evolving. It was found that the drive mechanism is the incoherent emission from microscopic fluctuations. The beat mode was found to be driven by this mechanism so as to produce a seed island for the tearing mode. Any nonlinearity in the dynamical equations of the vorticity, Ohm's law, the parallel flow of ions, and ion energy was found to induce the nonlinear acceleration of the growth of the tearing mode in the direct simulation. Thus, clear evidence for the important interaction between the global plasma dynamics and microscopic turbulence was demonstrated. The size of the seed island, induced by the microscopic turbulence, reached the range of a few percent in comparison with the width of the saturated island in the simulation. It is emphasized that the incoherent emission by the microscopic fluctuations makes an important contribution to seeding the magnetic island for the tearing mode evolution. This analysis has provided a basis for direct simulation to verify the hypothesis that incoherent nonlinear interaction works as the kick for exciting the tearing mode. The influence on the threshold amplitude necessary to enter the Rutherford regime was also studied. It was found that, due to the accelerated growth, the threshold amplitude necessary to enter the Rutherford regime becomes higher. This becomes prominent if the plasma temperature increases and the magnetic Reynolds number increases.

It should be noticed that in this paper we have analyzed the role of incoherent interaction, because of the relevance of such cases as demonstrated by direct simulations. More general consideration will be necessary in order to completely identify the role of microscopic fluctuations on the evolution of the tearing mode. Following the WTT formalism, Eq. (17) is deduced into the form

$$\frac{\partial}{\partial t} I_k + L_k I_k = \sum_{k'} A_{kk'} I_{k'} I_k + \sum_{k'} B_{kk'} I_{k'} I_{k-k'}, \quad (42)$$

where the $\sum_{k'} A_{kk'} I_{k'} I_k$ term is not retained in the analysis of this article. The first term on the right hand indicates the term that shows a coherent interaction on the test mode. This effect appears as a possible influence of the anomalous resistivity, turbulent thermal conductivity, and turbulent viscosity. The effective turbulent resistivity and viscosity can change sign such as in the cases of zonal field and zonal flow [4]. In the present problem, i.e., the excitation of the tearing mode by background turbulence, the second term, the incoherent interaction, plays the dominant role. The case where the first term in the RHS of Eq. (42) is important has been discussed in, e.g.,[18]. These findings illustrate the important roles of microscopic turbulence on the evolution of global perturbations, the integrated analyses of which require future intensive studies.

Acknowledgements

This work is partly supported by a Grant-in-Aid for Specially-Promoted Research from MEXT (16002005), by a Grant-in-Aid for Scientific Research from JSPS (19360415), and by the collaboration programs of NIFS and of the Research Institute for Applied Mechanics of Kyushu University, by Asada Science Foundation, and by the U.S. DOE under Grant No FG02-04ER54738. One of the authors (PHD) acknowledges the hospitality of Kyushu University.

Appendix. Weak Turbulence Formalism and Nonlinear Source Term

The set of model equations (17)

$$\frac{\partial}{\partial t}\boldsymbol{X} + \boldsymbol{L}\boldsymbol{X} = \boldsymbol{N}$$

is rewritten after the diagonalization as

$$-i\omega_{\mathrm{b}}\boldsymbol{Y}_k + \boldsymbol{D}_k\boldsymbol{Y}_k = \boldsymbol{M}_k. \quad (A1)$$

Keeping the least-stable response $Y_{1,k}$, we solve the equation for $Y_{1,k}$:

$$-i\omega_{\mathrm{b}}Y_{1,k} + D_{11,k}Y_{1,k} = M_{1,k}. \quad (A2)$$

The response is given as

$$\left|Y_{1,k}\right|^2 = \frac{\left|M_{1,k}\right|^2}{\left(\mathrm{Im}\, D_{11,k} - \mathrm{Re}\,\omega_{\mathrm{b}}\right)^2 + \left(\mathrm{Re}\, D_{11,k} + \gamma_{\mathrm{b}}\right)^2}, \quad (A3)$$

where $\gamma_{\mathrm{b}} = \mathrm{Im}\,\omega_{\mathrm{b}}$. According to a standard procedure of the weak turbulence theory [14], the relation

$$\left((\omega - \omega_k)^2 + \gamma_k^2\right)^{-1} = \pi|\gamma_k|^{-1}\delta(\omega - \omega_k)$$

is employed, and Eq. (A3) yields the result

$$\frac{\partial}{\partial t} I_k + \mathrm{Re}\, D_{11,k} I_k = \pi |M_{1,k}|^2, \quad (A4)$$

where $I_k = \int \left|Y_{1,k}\right|^2 \mathrm{d}\omega$.

Interpretation of the field variable $\boldsymbol{X}_k$ from the amplitude $Y_{1,k}$ is straightforward. Here, we take an approximation that the more strongly damped eigenmodes $Y_{n,k}\,(n = 2, 3, 4)$ are neglected in comparison with the least stable component, $Y_{1,k}$. Thus, one has $\boldsymbol{X}_k = \boldsymbol{U}^{-1}\boldsymbol{y}_k$, where $\boldsymbol{y}_k = (Y_{1,k}, 0, 0, 0)^{\mathrm{T}}$. Therefore, once the amplitude $Y_{1,k}$ is obtained, the partition among $X_{m,k}\,(m = 1, 2, 3, 4)$ is given immediately.

Next, the nonlinear driving term $M_{1,k} = \sum_{j=1}^{4} U_{1j}N_j$ is evaluated for a simplified expression of Eq. (24)

$$\left|M_{1,k}\right|^2 = \left|U_{14,k}\right|^2 \left|N_{4,k}\right|^2.$$

For the case where N_4 is taken into account, the combination $X_{1,k-k'}X_{4,k'}$ appears, and Eq. (25) gives

$$\left|N_{4,k}\right|^2 = \left\langle \sum_{k'\omega'k''\omega''} V_{k-k',k'} V^*_{k-k'',k''} \times X_{j,k-k'} X_{j',k'} X^*_{j,k-k''} X^*_{j',k''} \right\rangle. \quad (A5)$$

By employing a random phase approximation (RPA), the right hand side remains for the combination of $k' = k''$ or $k' = k'' - k$.

$$\left|N_{4,k}\right|^2 = \left\langle \sum_{k'\omega'} \left|V_{k-k',k'}\right|^2 \left|X_{j',k'}\right|^2 \left|X_{j,k-k'}\right|^2 \right\rangle + \sum_{k'\omega'} V_{k-k',k'} V^*_{-k',k-k'} \left\langle X_{j,k-k'} X^*_{j',k-k'} \right\rangle \left\langle X_{j',k'} X^*_{j,k'} \right\rangle. \quad \text{(A6)}$$

In the case that $|k'| \gg |k|$, the right hand side is evaluated by the leading term of $k \to 0$, i.e.,

$$\left|N_{4,k}\right|^2 \simeq \sum_{k'\omega'} \left|V_{k',k'}\right|^2 \left|X_{j',k'}\right|^2 \left|X_{j,k'}\right|^2 + \sum_{k'\omega'} V_{k',k'} V^*_{-k',-k'} \left\langle X_{j,k'} X^*_{j',k'} \right\rangle \left\langle X_{j',k'} X^*_{j,k'} \right\rangle. \quad \text{(A7)}$$

If one employs the case that $X_{j,k'}$ and $X_{j',k'}$ are in phase (such as the density and potential perturbation in drift wave fluctuations), one has a simplified expression as

$$\left|N_{4,k}\right|^2 \simeq 2 \sum_{k'\omega'} \left|V_{k',k'}\right|^2 \left|X_{j',k'}\right|^2 \left|X_{j,k'}\right|^2. \quad \text{(A8)}$$

This provides the formula

$$\left|M_{1,k}\right|^2 \simeq 2 \left|U_{14,k}\right|^2 \sum_{k'\omega'} \left|V_{k',k'}\right|^2 \left|X_{j',k'}\right|^2 \left|X_{j,k'}\right|^2 \quad \text{(A9)}$$

[1] J.D. Callen *et al.*, in Fusion Energy 1986 (Proc. 11th Int. Conf. Kyoto, 1986), vol.2 IAEA, Vienna (1987).

[2] A.I. Smolyakov, Plasma Phys. Control. Fusion **35**, 657 (1993).

[3] M. Yagi *et al.*, in Fusion Energy 2002 (Proc. 19th Int. Conf. Lyon, 2002) (Vienna: IAEA) CD-ROM file TH/1-4 and http://www.iaea.org/programmes/ripc/physics/fec2002 /html/fec2002.htm

[4] P.H. Diamond, S.-I. Itoh, K. Itoh and T.S. Hahm, Plasma Phys. Control. Fusion **47**, R35 (2005).

[5] M. Yagi, S. Yoshida, S.-I. Itoh, H. Naitou, H. Nagahara *et al.*, Nucl. Fusion **45**, 900 (2005).

[6] A. Furuya, M. Yagi and S.-I. Itoh, J. Phys. Soc. Jpn. **72**, 313 (2003).

[7] O.J. Kwon, P.H. Diamond and H. Biglari, Phys. Fluids B **2** 291 (1990).

[8] S.I. Braginskii, *Reviews of Plasma Physics*, ed. M.A. Leontovich (Consultant Bureau, New York, 1965) Vol.1.

[9] R.D. Hazeltine, M. Kotschenreuther and P.J. Morrison, Phys. Fluids **28**, 2466 (1985).

[10] B. Scott, Plasma Phys. Control. Fusion **39**, 471 (1997).

[11] S.P. Hirshman and D.J. Sigmar, Nucl. Fusion **21**, 1079 (1981).

[12] J.D. Callen and K.C. Shaing, Phys. Fluids **28**, 1845 (1985).

[13] T. Hayashi, Master thesis (Kyushu University, February 2007).

[14] B.B. Kadomtsev, *Plasma Turbulence* (Academic Press, New York, 1965).

[15] S.-I. Itoh, K. Itoh and M. Yagi, Phys. Rev. Lett. **91**, 045003 (2003).

[16] S.-I. Itoh, K. Itoh and M. Yagi, Plasma Phys. Control. Fusion **46**, 045003 (2004).

[17] P.H. Rutherford, Phys. Fluids **16**, 1903 (1973).

[18] C.J. McDevitt and P.H. Diamond, Phys. Plasmas **13**, 032302 (2006).